Journal of Applied Mechanics and Technical Physics, Vol. 38, No. 3, 1997

NUMERICAL MODEL OF THE DYNAMICS OF A MOMENTUMLESS TURBULENT WAKE IN A PYCNOCLINE

O. F. Voropayeva and G. G. Chernykh

UDC 532.517.4

1. Introduction. Turbulent wakes behind bodies of revolution in a stratified fluid have been considered in many publications [1–21]. In [1], Schooley and Steward have analyzed experimentally the dynamics of a turbulent wake behind a self-propelled body in a linearly stratified medium. In addition, they have demonstrated collapse and generation by the wake of internal waves. The phenomenon of momentumless wake collapse in a linearly stratified medium has been studied experimentally by Merrit in [2]. In laboratory tests, Lin and Pao [3] (see also [4]) have investigated in detail the turbulence characteristics in the wakes behind bodies moving in a linearly stratified medium. In [5], Gilreath and Brandt have analyzed experimentally the pattern of internal waves generated during the motion of bodies in stratified fluids. In addition, they have given theoretical estimates of internal waves, including the waves induced by the collapse of the turbulent wake in pycnocline.

A series of studies [6–13] deals with the flow occurring during motion of a towed sphere in a linearly stratified fluid. Various flow regimes have been studied, depending on the Reynolds and Froude numbers both in the near and far wakes. In [10], Bonneton et al. have studied theoretically internal waves produced by the turbulent wake of a sphere moving in a linearly stratified fluid. In addition, they have considered the wake's wave component that is associated with coherent structures. In [12, 14], Chashechkin and Voisin have comprehensively analyzed experimental data on turbulent-wake degeneration behind towed and self-propelled bodies in linearly stratified fluids and also have estimated theoretically the parameters of internal waves.

The initial stage of development of the wake in a linearly stratified fluid has been considered theoretically by Onufriev [15] using the algebraic model of Reynolds stresses and fluxes. In [16], Lewellen et al. have modeled numerically the turbulent wake and collapse-produced internal waves at small distances from a self-propelled body in a linearly stratified medium, which is based on the model of a local-equilibrium approach.

To analyze numerically the wakes behind self-propelled and towed bodies in a linearly stratified medium, Hassid [4] used a modified model of the locally equilibrium approach with involvement of the equations of turbulent-energy transfer and its dissipation rate. He obtained satisfactory agreement with the experimental data obtained by Lin and Pao which are concerned with the measurement of the characteristic sizes of the wake, velocity defect, and turbulence energy on the wake axis as a function of the distance from a body (for one of the values of the Froude number). However, as correctly noted in [22], for a self-propelled body, the action of stratification turned out to be stronger than in experiments.

As an illustration of application of the implicit variant of the splitting method in terms of physical processes for stratified-flow calculations, Danilenko et al. [17] have considered the turbulent wake behind a self-propelled body in a linearly stratified fluid. The studies [18–21] also deal with a numerical modeling of turbulent wakes behind bodies in stratified fluids. In particular, the role of the initial swirling in the evolution of a momentumless turbulent wake in a linearly stratified medium was evaluated by Glushko et al. [19]. Chernykh et al. [20, 21] have analyzed a variant of the momentumless wake in a fluid with nonlinear density distribution in depth. For linear stratification, they obtained satisfactory agreement with the experimental data in [3] on the anisotropic decay of the intensities of turbulent velocity-field fluctuations.

Institute of Computational Technologies, Siberian Division, Russian Academy of Sciences, Novosibirsk 630090. Translated from Prikladnaya Mekhanika i Tekhnicheskaya Fizika, Vol. 38, No. 3, pp. 69–86, May–June, 1997. Original article submitted October 20, 1995; revision submitted December 20, 1995.

0021-8944/97/3803-0391 $18.00

In [2, 23–26], turbulent wakes have been studied using a schematic plane model. The plane nonstationary problem of the evolution of the localized-perturbation region in a linearly stratified fluid has been considered. Some studies [27–30] are devoted to the dynamics of localized plane regions of a turbulent fluid in media with nonlinear stratification.

A simple analytical quasi-one-dimensional model of the evolution of the turbulent-perturbation region in the wake behind a body moving in a linearly stratified medium was constructed in [31].

In the analysis of the literature cited above, we should mention the following. Degeneration of momentumless turbulent wakes in a linearly stratified fluid has been fairly well studied. Both experimental and consistent calculational-theoretical modeling results are available.

In the case of nonlinear stratification, the situation is more complicated, because data of laboratory experiments on degeneration of the turbulent wake proper are practically absent.

The calculation results given in [28, 29] were obtained based on the schematic plane model. In this case, the question on the role of the defect of the horizontal velocity component toward a direction that coincides with the direction of body motion remains open. In addition, there is no correspondence with the results of the laboratory experiments in [3] for a homogeneous fluid. The pycnocline plays a special part among the nonlinear density distributions of an unperturbed fluid in depth. In this case, a pattern of finite-amplitude internal waves which is close to a steady-state one can be formed [5, 25]. In the publications known to the authors, there are no results of numerical modeling of the dynamics of a momentumless turbulent wake in a pycnocline. In the present work, we make an attempt to investigate numerically this flow with application of a modified e–ε model of turbulence.

2. Formulation of the Problem. *Governing Equations.* To describe the flow in the far turbulent wake behind a body of revolution in a stratified medium, we use the following system of averaged equations of motion, continuity, and incompressibility in the Oberbeck–Boussinesq approach:

$$U_\infty \frac{\partial U_D}{\partial x} + V\frac{\partial U_D}{\partial y} + W\frac{\partial U_D}{\partial z} = \frac{\partial}{\partial y}\langle u'v'\rangle + \frac{\partial}{\partial z}\langle u'w'\rangle; \tag{2.1}$$

$$U_\infty \frac{\partial V}{\partial x} + V\frac{\partial V}{\partial y} + W\frac{\partial V}{\partial z} = -\frac{1}{\rho_0}\frac{\partial\langle p_1\rangle}{\partial y} - \frac{\partial}{\partial y}\langle v'^2\rangle - \frac{\partial}{\partial z}\langle v'w'\rangle; \tag{2.2}$$

$$U_\infty \frac{\partial W}{\partial x} + V\frac{\partial W}{\partial y} + W\frac{\partial W}{\partial z} = -\frac{1}{\rho_0}\frac{\partial\langle p_1\rangle}{\partial z} - \frac{\partial}{\partial y}\langle v'w'\rangle - \frac{\partial}{\partial z}\langle w'^2\rangle - g\frac{\langle\rho_1\rangle}{\rho_0}; \tag{2.3}$$

$$U_\infty \frac{\partial\langle\rho_1\rangle}{\partial x} + V\frac{\partial\langle\rho_1\rangle}{\partial y} + W\frac{\partial\langle\rho_1\rangle}{\partial z} + W\frac{d\rho_s}{dz} = -\frac{\partial}{\partial y}\langle v'\rho'\rangle - \frac{\partial}{\partial z}\langle w'\rho'\rangle; \tag{2.4}$$

$$\frac{\partial V}{\partial y} + \frac{\partial W}{\partial z} = 0. \tag{2.5}$$

Here $U_D = U_\infty - U$ is the defect of the averaged longitudinal velocity component; U, V, and W are the velocity components of the averaged motion in the direction of the x, y, and z axes; p_1 is the deviation of the pressure from hydrostatic pressure, which is due to the stratification $\rho_s(z)$, U_∞ is the free-stream velocity; g is the acceleration of gravity, $\langle\rho_1\rangle$ is the averaged density defect: $\rho_1 = \rho - \rho_s$; $\rho_s = \rho_s(z)$ is the density of the unperturbed fluid: $d\rho_s/dz \leqslant 0$ (stable stratification); $\rho_0 = \rho_s(0)$; the prime and $\langle\ \rangle$ refer to the pulsation components and averaging, respectively. The system of coordinates is related to a moving body such that the velocity of motion of this body is equal to $-U_\infty$, and the z axis is directed vertically upward, against the gravity. The fluid density is assumed to be a linear function of temperature, and stratification is assumed to be weak. On the right-hand sides of Eqs. (2.1)–(2.4), terms which contain the derivative with respect to the variable x and also cofactors as a laminar-viscosity or diffusion coefficient are omitted under the assumption that these terms are small. As in [4], the term $\partial U/\partial x$ in (2.5) is omitted under the assumption of its smallness. The authors based the last simplification on the arguments of [4], the essence of which lies in the fact that system (2.1)–(2.5) is equivalent to the system of equations of the far wake in a homogeneous fluid; for this case, $V = W \approx 0$ and Eqs. (2.2), (2.3), and (2.5) are not considered. In the case of the wake dynamics in a stratified fluid, a convective flow corresponding to wake-generated internal waves emerges in the (y, z) plane.

Degeneration of the velocity components V, and W occurs more slowly than degeneration of $U_D = U_\infty - U$. This assertion seems plausible for the momentumless wakes that we are considering in the present study. In addition, in [20] the authors performed numerical experiments in which, for one of the variants of the problem parameters, degeneration of the momentumless turbulent wake in a stratified medium is modeled numerically using both the complete three-dimensional equation of incompressibility and its simplified variant (2.5). The calculation results proved to be fairly close. Following from the foregoing considerations, the authors (precisely as the authors of [4, 19]) used the equation of incompressibility in the form of (2.5). Application of (2.5) simplified considerably the numerical algorithm for the solution of the problem. System (2.1)–(2.5) is different from that adopted in [4] by the absence of the quantity $\partial\langle p_1\rangle/\partial x$ in Eq. (2.1).

Model of Turbulent Motion. System (2.1)–(2.5) is not closed. In the present work, the components of the Reynolds-stress tensor $\langle u_i' u_j'\rangle$ (except for $\langle v'w'\rangle = \langle u_2' u_3'\rangle$), turbulent fluxes $\langle u_i'\rho'\rangle$, and of the dispersion of the density fluctuations $\langle \rho'^2\rangle$ are approximated by the relations of [32] (summation is performed over repeated indices):

$$\frac{\langle u_i' u_j'\rangle}{e} = \frac{2}{3}\delta_{ij} + \frac{1-c_2}{c_1}\left(\frac{P_{ij}}{\varepsilon} - \frac{2}{3}\delta_{ij}\frac{P}{\varepsilon}\right) + \frac{1-c_3}{c_1}\left(\frac{G_{ij}}{\varepsilon} - \frac{2}{3}\delta_{ij}\frac{G}{\varepsilon}\right); \tag{2.6}$$

$$-\langle u_i'\rho'\rangle = \frac{e}{c_{1T}\varepsilon}\left[\langle u_i' u_k'\rangle\frac{\partial\langle\rho\rangle}{\partial x_k} + (1-c_{2T})\left(\langle u_k'\rho'\rangle\frac{\partial U_i}{\partial x_k} - \frac{g_i}{\rho_0}\langle\rho'^2\rangle\right)\right]; \tag{2.7}$$

$$\langle\rho'^2\rangle = -\frac{2}{c_T}\frac{e}{\varepsilon}\langle u_k'\rho'\rangle\frac{\partial\langle\rho\rangle}{\partial x_k}; \tag{2.8}$$

$$P_{ij} = -\left\{\langle u_i' u_k'\rangle\frac{\partial U_j}{\partial x_k} + \langle u_j' u_k'\rangle\frac{\partial U_i}{\partial x_k}\right\}, \quad G_{ij} = \frac{1}{\rho_0}\left(\langle u_i'\rho'\rangle g_j + \langle u_j'\rho'\rangle g_i\right). \tag{2.9}$$

Here i, j, and k can take on the values 1, 2, and 3, $\mathbf{g} = (0, 0, -g)$, $2P = P_{ii}$, $2G = G_{ii}$, $U_1 = U$, $U_2 = V$, and $U_3 = W$.

Similarly to [4], we shall simplify expressions (2.6)–(2.9) with allowance for the specific physical features of the flow considered — concurrent jet turbulent flow in the gravity field at large distances from the body. In this case, relations (2.9) are replaced by approximate ones:

$$P_{11} = 2\left(\langle u'v'\rangle\frac{\partial U_D}{\partial y} + \langle u'w'\rangle\frac{\partial U_D}{\partial z}\right), \quad P_{22} = P_{33} = 0, \quad P_{12} = \langle v'^2\rangle\frac{\partial U_D}{\partial y}, \quad P_{13} = \langle w'^2\rangle\frac{\partial U_D}{\partial z}.$$

Expressions (2.6)–(2.8) are simplified as follows:

$$\langle u'v'\rangle = \frac{1-c_2}{c_1}\frac{e\langle v'^2\rangle}{\varepsilon}\frac{\partial U_D}{\partial y} = K_y\frac{\partial U_D}{\partial y}; \tag{2.10}$$

$$\langle u'w'\rangle = (1-c_2)e\langle w'^2\rangle\Big/\left[c_1\varepsilon\left(1 - \frac{1-c_3}{c_1 c_{1T}}\frac{g}{\rho_0}\frac{e^2}{\varepsilon^2}\frac{\partial\langle\rho\rangle}{\partial z}\right)\right]\frac{\partial U_D}{\partial z} = K_z\frac{\partial U_D}{\partial z}; \tag{2.11}$$

$$\langle\rho'^2\rangle = -\frac{2}{c_T}\frac{e}{\varepsilon}\langle w'\rho'\rangle\frac{\partial\langle\rho\rangle}{\partial z}; \tag{2.12}$$

$$-\langle v'\rho'\rangle = \frac{e\langle v'^2\rangle}{c_{1T}\varepsilon}\frac{\partial\langle\rho\rangle}{\partial y} = K_{\rho y}\frac{\partial\langle\rho\rangle}{\partial y}; \tag{2.13}$$

$$-\langle w'\rho'\rangle = \frac{e}{c_{1T}\varepsilon}\left[\langle w'^2\rangle\frac{\partial\langle\rho\rangle}{\partial z} + (1-c_{2T})\frac{g}{\rho_0}\langle\rho'^2\rangle\right]$$

$$= e\langle w'^2\rangle\Big/\left[c_{1T}\varepsilon\left(1 - 2\frac{1-c_{2T}}{c_{1T}c_T}\frac{g}{\rho_0}\frac{e^2}{\varepsilon^2}\frac{\partial\langle\rho\rangle}{\partial z}\right)\right]\frac{\partial\langle\rho\rangle}{\partial z} = K_{\rho z}\frac{\partial\langle\rho\rangle}{\partial z}. \tag{2.14}$$

The values of the turbulence energy e, the dissipation rate ε, and of the shear Reynolds stress $\langle v'w'\rangle$

are determined from the differential equations of transfer:

$$U_\infty \frac{\partial e}{\partial x} + V \frac{\partial e}{\partial y} + W \frac{\partial e}{\partial z} = \frac{\partial}{\partial y} K_{ey} \frac{\partial e}{\partial y} + \frac{\partial}{\partial z} K_{ez} \frac{\partial e}{\partial z} + P + G - \varepsilon; \tag{2.15}$$

$$U_\infty \frac{\partial \varepsilon}{\partial x} + V \frac{\partial \varepsilon}{\partial y} + W \frac{\partial \varepsilon}{\partial z} = \frac{\partial}{\partial y} K_{\varepsilon y} \frac{\partial \varepsilon}{\partial y} + \frac{\partial}{\partial z} K_{\varepsilon z} \frac{\partial \varepsilon}{\partial z} + c_{\varepsilon 1} \frac{\varepsilon}{e}(P + G) - c_{\varepsilon 2} \frac{\varepsilon^2}{e}; \tag{2.16}$$

$$U_\infty \frac{\partial \langle v'w' \rangle}{\partial x} + V \frac{\partial \langle v'w' \rangle}{\partial y} + W \frac{\partial \langle v'w' \rangle}{\partial z} = \frac{\partial}{\partial y} K_{ey} \frac{\partial \langle v'w' \rangle}{\partial y} + \frac{\partial}{\partial z} K_{ez} \frac{\partial \langle v'w' \rangle}{\partial z} + (1 - c_2) P_{23}$$

$$+ (1 - c_3) G_{23} - c_1 \frac{\varepsilon}{e} \langle v'w' \rangle \qquad \left(P_{23} = -\left\{ \langle v'^2 \rangle \frac{\partial W}{\partial y} + \langle w'^2 \rangle \frac{\partial V}{\partial z} \right\}, \quad G_{23} = -\frac{g}{\rho_0} \langle v'\rho' \rangle \right). \tag{2.17}$$

The turbulent-viscosity coefficients in Eqs. (2.15)–(2.17) have the form [32]

$$K_{ey} = c_s e \langle v'^2 \rangle / \varepsilon, \quad K_{ez} = c_s e \langle w'^2 \rangle / \varepsilon, \quad K_{\varepsilon y} = K_{ey}/\sigma, \quad K_{\varepsilon z} = K_{ez}/\sigma. \tag{2.18}$$

After these manipulations, the mathematical model of the far turbulent wake is the system of differential equations (2.1)–(2.5), (2.15)–(2.17) with allowance for (2.10), (2.11), (2.13), (2.14), and (2.18). The quantity $\langle \rho'^2 \rangle$ is determined by the algebraic relation (2.12); $c_1 = 2$, $c_2 = 0.6$, $c_3 = 0.6$, $c_{1T} = 3.2$, $c_{2T} = 0.5$, $c_T = 1.25$, $c_{\varepsilon 1} = 1.44$, $c_{\varepsilon 2} = 1.92$, $c_s = 0.22$, and $\sigma = 1.3$ are empirical constants. The main difference of this mathematical model from that adopted in [4] lies in the use of "isotropic" [32] relations (2.6) in order to determine the components of the Reynolds-stress tensor instead of a locally equilibrium approximation. Approximation (2.6) in the present work allowed one to obtain a better correspondence of the calculation results to the experimental results obtained by Lin and Pao [4] in a linearly stratified fluid.

Initial and Boundary Conditions. The variable x in Eqs. (2.1)–(2.4) and (2.15)–(2.17) plays the role of time. For $x = x_0$, the following initial conditions were specified:

$$U_D(x_0, y, z) = \theta_0(r), \quad e(x_0, y, z) = \theta_1(r), \quad \varepsilon(x_0, y, z) = \theta_2(r), \quad r^2 = y^2 + z^2 \quad (0 \leqslant r < \infty),$$

$$\langle \rho_1 \rangle = V = W = \langle v'w' \rangle = 0 \quad (-\infty < y < \infty, \quad -\infty < z < \infty, \quad x = x_0).$$

Here $\theta_0(r)$, $\theta_1(r)$, and $\theta_2(r)$ are finite bell-shaped functions which are consistent with the experimental data obtained in a homogeneous fluid.

For $r \to \infty$, the following unperturbed-flow conditions were set:

$$U_D = e = \varepsilon = \langle v'w' \rangle = \langle \rho_1 \rangle = V = W = 0. \tag{2.19}$$

We have also considered the distributions $\rho_s(z)$ such that the function $\rho_s(z) - \rho_0$ is an antisymmetric function of z. In this case, from the symmetry considerations, the solution was searched only in the first quadrant of the plane (y, z) with the use of boundary conditions in the form

$$\frac{\partial \langle \rho_1 \rangle}{\partial y} = \frac{\partial e}{\partial y} = \frac{\partial \varepsilon}{\partial y} = V = \frac{\partial W}{\partial y} = \frac{\partial U_D}{\partial y} = \langle v'w' \rangle = 0 \quad (y = 0, \quad z \geqslant 0),$$

$$\langle \rho_1 \rangle = \frac{\partial e}{\partial z} = \frac{\partial \varepsilon}{\partial z} = W = \frac{\partial V}{\partial z} = \frac{\partial U_D}{\partial z} = \langle v'w' \rangle = 0 \quad (z = 0, \quad y \geqslant 0).$$

In numerical solution of the problem, the boundary conditions (2.19), which correspond to $r \to \infty$, were referred to the boundaries of the large rectangle $z = z_*$ $(0 \leqslant y \leqslant y_*)$ and $y = y_*$ $(0 \leqslant z \leqslant z_*)$.

It is convenient to reduce system (2.2), (2.3), and (2.5) to the following:

$$U_\infty \frac{\partial \omega}{\partial x} + V \frac{\partial \omega}{\partial y} + W \frac{\partial \omega}{\partial z} = \frac{g}{\rho_0} \frac{\partial \langle \rho_1 \rangle}{\partial y} - \frac{\partial^2}{\partial y \partial z} \left[\langle v'^2 \rangle - \langle w'^2 \rangle \right] - \frac{\partial^2}{\partial z^2} \langle v'w' \rangle + \frac{\partial^2}{\partial y^2} \langle v'w' \rangle; \tag{2.20}$$

$$\frac{\partial^2 \psi}{\partial y^2} + \frac{\partial^2 \psi}{\partial z^2} = \omega. \tag{2.21}$$

Here the stream function ψ is defined by the equalities $V = \partial\psi/\partial z$ and $W = -\partial\psi/\partial y$.

Nondimensionalization. The variables of the problem can be made nondimensional with the use of the scale of length D (body diameter) and the scale of velocity U_∞ (unperturbed-flow velocity). Let us introduce the following nondimensional variables:

$$x^* = x/D, \quad y^* = y/D, \quad z^* = z/D, \quad U_i^* = U_i/U_\infty, \quad \langle u_i' u_j' \rangle^* = \langle u_i' u_j' \rangle / U_\infty^2,$$
$$e^* = e/U_\infty^2, \quad \varepsilon^* = \varepsilon D/U_\infty^3, \quad \langle \rho_1 \rangle^* = \langle \rho_1 \rangle/(aD\rho_0), \quad \langle u_i' \rho' \rangle^* = \langle u_i' \rho' \rangle/(aD\rho_0 U_\infty),$$
$$\langle \rho'^2 \rangle^* = \langle \rho'^2 \rangle/(aD\rho_0)^2 \quad [a = -(1/\rho_0) d\rho_s/dz, \quad z = 0].$$

As a result, in the nondimensional equations, the quantity $4\pi^2/\mathrm{Fr}^2$ appears instead of g, where Fr is the Froude number determined by the equality $\mathrm{Fr} = U_\infty T/D$ ($T = 2\pi/\sqrt{ag}$ is the Brunt–Väisälä period). To interpret the calculation results, it is appropriate to introduce the time t connected with the distance from the body: $t = x/U_\infty$, $t^* = t/T = xD/(U_\infty DT) = x^*/\mathrm{Fr}$. In what follows, the superscript of nondimensionalization (asterisk) is omitted everywhere except for the figures.

3. Algorithm for Solution of the Problem. To construct a finite-difference algorithm, we shall introduce the following new independent variables:

$$x' = x, \quad \xi = y' = \chi_1(y), \quad \eta = z' = \chi_2(z) \quad [x = x', \quad y = \varphi_1(\xi), \quad z = \varphi_2(\eta)]. \tag{3.1}$$

The Jacobian of the transformation that performs a transition from variables (x, y, z) to variables (x', y', z') is as follows:

$$J = \frac{\partial(x, y, z)}{\partial(x', \xi, \eta)} = \frac{\partial y}{\partial \xi} \frac{\partial z}{\partial \eta}.$$

The functions φ_1 and φ_2 are given in a tabular form; their choice enabled us to cluster the grid nodes in the domain of large density gradients and in the vicinity of the turbulent wake. In the new coordinate system (x', ξ, η), the nodes of the calculation grid in the plane (ξ, η) are distributed uniformly: $\xi_i = i\Delta\xi$ and $\eta_j = j\Delta\eta$ $(i = 0, \ldots, M_1;\ j = 0, \ldots, M_2)$, $\varphi_1(\xi_{M_1}) = y_*$, and $\varphi_2(\eta_{M_2}) = z_*$. The grid step Δx in the direction of the x axis was chosen variable.

The algorithm for solving the problem was reduced to a successive integration of system of equations (2.20), (2.21), (2.1), (2.4), and (2.15)–(2.17) which are written in the new coordinate system, in each layer n over the variable x. This algorithm is based on the method of splitting in terms of spatial variables [33]. To solve the equation of vorticity transfer (2.20), we use the simplest splitting scheme with approximation of convective terms by one-sided upwind differences. The values of the stream function ψ were calculated using the iteration scheme of stabilizing correction.

The remaining equations of the mathematical model were integrated using the method of splitting in terms of spatial variables, and convective terms were approximated by central-difference relations. Because of the awkwardness, the finite-difference analogs of these equations are not given here. The equations were integrated successively by the scalar sweep method. In computations of any of the functions ψ, U_D, $\langle \rho_1 \rangle$, e, ε, and $\langle v'w' \rangle$ on the layer $(n + 1)$, we used the already known quantities (functions) on this layer, while the rest of them were taken from the lower layer n. Thus, recalling the simplicity of a computer realization, we took advantage of the idea of a "block" analog of the Seidel method.

We shall dwell on the approximation of the boundary conditions. The challenge is symmetry conditions for the defect of the longitudinal velocity component U_D. Since we consider the momentumless turbulent flow, the law of conservation is a consequence of the integration of Eq. (2.1) over the entire cross section:

$$\iint_{-\infty}^{\infty} U_D \, dy \, dz = \iint_{-\infty}^{\infty} U_D(x_0, y, z) \, dy \, dz = \iint_{-\infty}^{\infty} J U_D(x_0, \xi, \eta) \, d\xi \, d\eta = I_0 = 0. \tag{3.2}$$

As already noted, for numerical integration of Eq. (2.1), the scheme of splitting in terms of spatial variables was employed. A scheme in integer steps, which is equivalent to it, contains terms of the order $O(\Delta x)$ which are absent in the implicit finite-difference scheme, which is a direct approximation of (2.1). Along with the central-difference approximations of convective terms in Eq. (2.1), these terms turn out to be inconsistent

with the approximation of the Neumann conditions on the axes of symmetry in the sense that the analog of the conservation law (3.2) is satisfied in the first quadrant of the plane (ξ, η). Since the coordinate axes can be regarded as the boundary of the region only conditionally, the finite-difference equations on the integral and fractional steps were solved up to the boundary with the use of the symmetry (antisymmetry) conditions of the form (the superscript n refers to the variable x'):

$$(U_D)^{n+1/2}_{-1,j} = (U_D)^{n+1/2}_{1,j}, \quad e^n_{-1,j} = e^n_{1,j}, \quad \varepsilon^n_{-1,j} = \varepsilon^n_{1,j}, \quad \psi^{n+1}_{-1,j} = -\psi^{n+1}_{1,j} \quad (0 \leqslant j \leqslant M_2),$$
$$(U_D)^{n+1}_{i,-1} = (U_D)^{n+1}_{i,1}, \quad e^n_{i,-1} = e^n_{i,1}, \quad \varepsilon^n_{i,-1} = \varepsilon^n_{i,1}, \quad \psi^{n+1}_{i,-1} = -\psi^{n+1}_{i,1} \quad (0 \leqslant i \leqslant M_1).$$

The consequence of such an approximation of the boundary conditions of symmetry and the splitting scheme used is the conservation law which is equivalent to the grid approximation (3.2):

$$I_{01} = \Bigg[\sum_{j=1}^{M_2-1} \sum_{i=1}^{M_1-1} J_{i,j}(U_D)^{n+1}_{i,j} + 0.5 \sum_{j=1}^{M_2-1} J_{0,j}(U_D)^{n+1}_{0,j}$$
$$+ 0.5 \sum_{i=1}^{M_1-1} J_{i,0}(U_D)^{n+1}_{i,0} + 0.25 J_{0,0}(U_D)^{n+1}_{0,0} \Bigg] \Delta\xi\Delta\eta = 0. \tag{3.3}$$

As the boundary conditions for e, ε, and $\langle\rho_1\rangle$, on the axes of coordinates we used conditions that are similar to the above ones, and the simplest approximations of the Neumann condition are as follows:

$$e^{n+1/2}_{0,j} = e^{n+1/2}_{1,j}, \quad \varepsilon^{n+1/2}_{0,j} = \varepsilon^{n+1/2}_{1,j}, \quad \langle\rho_1\rangle^{n+1/2}_{0,j} = \langle\rho_1\rangle^{n+1/2}_{1,j},$$
$$e^{n+1}_{i,0} = e^{n+1}_{i,1}, \quad \varepsilon^{n+1}_{i,0} = \varepsilon^{n+1}_{i,1}, \quad \langle\rho_1\rangle^{n+1}_{i,0} = 0 \quad (0 \leqslant i \leqslant M_1; \quad 0 \leqslant j \leqslant M_2).$$

In this case, the deviation of the grid solutions in a norm that is a grid analog of the space norm of continuous functions, did not exceed 6%.

Special attention was given to the approximation of the boundary conditions for Eq. (2.1) in connection with the fact that the nondivergence of the finite-difference algorithm [nonsatisfaction of (3.3)] can lead to a substantial distortion of the solution even in a homogeneous fluid [34].

4. Testing the Algorithm. Convergence of the algorithm was tested experimentally by solving model problems. In the case of a homogeneous fluid ($g = 0$), the initial differential problem is equivalent to the following system of one-dimensional equations:

$$\frac{\partial U_D}{\partial x} = \frac{1}{r}\frac{\partial}{\partial r}\left(rK\frac{\partial U_D}{\partial r}\right); \tag{4.1}$$

$$\frac{\partial e}{\partial x} = \frac{1}{r}\frac{\partial}{\partial r}\left(rK\frac{\partial e}{\partial r}\right) + P - \varepsilon; \tag{4.2}$$

$$\frac{\partial \varepsilon}{\partial x} = \frac{1}{r}\frac{\partial}{\partial r}\frac{rK}{\sigma}\frac{\partial \varepsilon}{\partial r} - c_{\varepsilon 2}\frac{\varepsilon^2}{e} + c_{\varepsilon 1}\frac{\varepsilon}{e}P, \tag{4.3}$$

where

$$K = \frac{1 - c_2}{c_1}\frac{\langle v'^2\rangle e}{\varepsilon}; \quad \langle v'^2\rangle = \frac{2}{3}e - \frac{2}{3}\frac{1 - c_2}{c_1}\frac{e}{\varepsilon}P; P = K\left(\frac{\partial U_D}{\partial r}\right)^2.$$

For $x = x_0 = 8$, we specified the initial conditions of [4] which are consistent with the experimental data of Lin and Pao on decay of turbulent wakes in a homogeneous fluid:

$$e(x_0, r) = E_0 \exp(-4r^2), \quad E_0 = e(x_0, 0), \quad \varepsilon(x_0, r) = \sqrt{12}\, E_0^{3/2} \exp(-6r^2),$$
$$U_D(x_0, r) = U_d(1 - 8r^2)\exp(-8r^2), \quad U_d = U_D(x_0, 0). \tag{4.4}$$

For $r = 0$, we set the following boundary conditions:

$$\frac{\partial e}{\partial r} = \frac{\partial \varepsilon}{\partial r} = \frac{\partial U_D}{\partial r} = 0. \tag{4.5}$$

For $r \to \infty$, the zero boundary conditions for the desired functions were specified.

Problem (4.1)–(4.5) was solved using the following finite-difference algorithm:

$$\frac{(U_D)_i^{n+1} - (U_D)_i^n}{\Delta x^n} = \frac{1}{r_i}(\Lambda U_D)_i^{n+1}; \tag{4.6}$$

$$\frac{e_i^{n+1} - e_i^n}{\Delta x^n} = \frac{1}{r_i}(\Lambda e)_i^{n+1} + P_i^{n+1} - \varepsilon_i^n; \tag{4.7}$$

$$\frac{\varepsilon_i^{n+1} - \varepsilon_i^n}{\Delta x^n} = \frac{1}{\sigma r_i}(\Lambda\varepsilon)_i^{n+1} - c_{\varepsilon 2}\varepsilon_i^{n+1}\varepsilon_i^n/e_i^{n+1} + c_{\varepsilon 1}\varepsilon_i^{n+1}P_i^{n+1}/e_i^{n+1} \tag{4.8}$$

$$(i = 1, \ldots, M_r - 1; \quad n = 0, \ldots, N).$$

Here $(\Lambda f)_i^{n+1} = (a_{i+1}f_{i+1}^{n+1} - (a_i + a_{i+1})f_i^{n+1} + a_i f_{i-1}^{n+1})/h_r^2$, $a_i = (r_i K_i^n + r_{i-1}K_{i-1}^n)/2$, $P_i^{n+1} = K_i^n(((U_D)_{i+1}^{n+1} - (U_D)_{i-1}^{n+1})/2h_r)^2$, and f is one of the functions U_D, e, and ε.

For the sake of simplicity, the grid step with respect to the variable r was assumed to be constant. The difference equations (4.6)–(4.8) are solved sequentially on each layer with respect to x. Problem (4.1)–(4.5) was integrated using the above finite-difference algorithm on the sequence of imbedded grids. The solutions were compared in the uniform norm. Calculations were performed on grids with the following parameters:

(1) $h_r^{(1)} = h_0 = 0.1$, $\tau_0^n = \Delta x^n = 0.01$–$0.5$ (τ_0^n was varied by the formula for the sum of terms of a arithmetical progression with difference 0.01);

(2) $h_r^{(2)} = h_0/2$ and $\tau_1^n = \tau_0^n/4$;

(3) $h_r^{(3)} = h_0/4$ and $\tau_2^n = \tau_0^n/8$;

(4) $h_r^{(4)} = h_0/8$ and $\tau_3^n = \tau_0^n/16$.

For $x = 100$, the relative difference of the solutions for two neighboring grids was 4.9, 1.1, and 0.35%, respectively, for the turbulence energy e; 4.05, 0.95, and 0.5% for the dissipation rate ε; and 5.8, 1.3, and 0.56% for U_D. These results show the convergence of the sequence of grid solutions in itself.

Further testing was conducted according to the following scheme: the grid solution that was obtained using a very fine grid ($\tau_3^n = \tau_0^n/16$ and $h_r^{(4)} = h_0/8$) was called an "exact" solution, and the algorithm of solution of the problem was tested as applied to Eqs. (2.1), (2.15), and (2.16). For simplicity, the transformation of coordinates (3.1) was assumed to be identical. Since system (2.1), (2.15), and (2.16) [and its one-dimensional analog (4.1)–(4.3)] is a system of degenerate parabolic equations [35] which possesses the property of finite perturbation velocity, it proved sufficient to set $y_* = 5$ and $z_* = 5$. A comparison yielded the following results. For $x = 100$ and the following parameters of a uniform calculation grid $\Delta x^n = \tau_0^n$ and $h_y = h_z = h_0$, $\Delta x^n = \tau_0^n/4$ and $h_y = h_z = h_0/2$, and $\Delta x^n = \tau_0^n/8$ and $h_y = h_z = h_0/4$, the relative deviations of the grid solutions of the two-dimensional problem from the "exact" solution for the turbulence energy e were 9.33, 6.8, and 6.09%, respectively. For the dissipation rate ε, the deviations obtained were equal to 8.8, 5.4, and 3.8%, and, for the velocity defect U_D, these quantities were equal to 14.4, 5.1, and 4.4%. To compare the "exact" solution of the one-dimensional problem (4.1)–(4.5) with that of its two-dimensional finite-difference analog, the values of the one-dimensional functions were restored in the nodes of the two-dimensional domain, using standard cubic spline-interpolation.

The problem of the anisotropic temperature wave [35] is a well-known test for solution algorithms of the two-dimensional nonlinear heat-conductivity equation. The authors checked the convergence of the algorithm (having changed one of the diffusion equations of the mathematical model) using this test as well.

In addition, the experimental analysis of convergence that we have made in the preceding consideration is of interest in connection with the fact that it is immediately connected with the problem to be solved and allows one to estimate the algorithm parameters, which must reach the given accuracy upon its solution in complete formulation.

The algorithm stage connected with integration of system (2.20), (2.21) was tested on the problem of the dynamics of a local density-field perturbation in a stratified medium [28].

The efficiency of the mathematical model in complete formulation was analyzed using the experimental

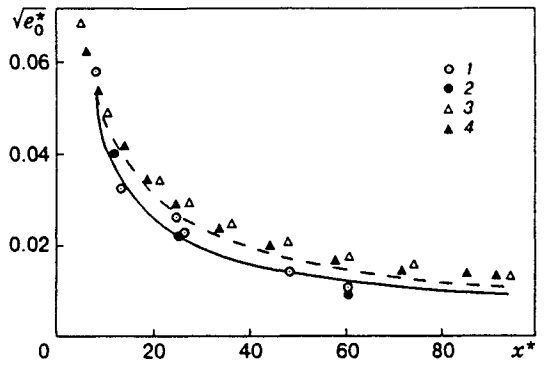

Fig. 1

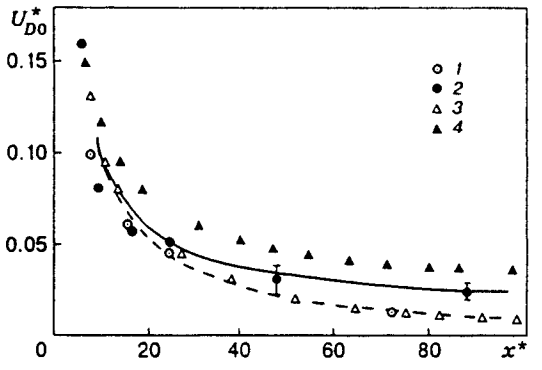

Fig. 2

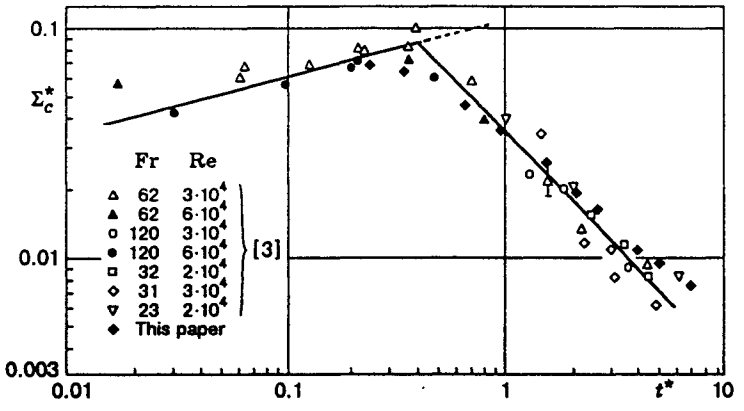

Fig. 3

data of Lin and Pao on degeneration of the momentumless turbulent wake in a linearly stratified medium [3, 4]. The calculation results for the Froude number Fr = 31 are given in Figs. 1–3. Figures 1 and 2 give the time variation of the axial values of the turbulence energy $e_0 = e_0(t) = e(t,0,0)$ and the velocity defect $U_{D0} = U_{D0}(t) = U_D(t,0,0)$. The dashed (homogeneous fluid) and solid (stratified fluid) curves show the results of this work, points 1 and 2 refer to the experimental data of Lin and Pao, and points 3 and 4 to the results of the numerical experiments performed by Hassid [4] (open points refer to a homogeneous fluid and filled points to a stratified fluid).

In Fig. 3, the calculated values of the density-fluctuation dispersion $\Sigma_c = \sqrt{\langle \rho'^2(t,0,0)\rangle}/\mathrm{Fr}^{1/4}$ are compared with the experimental data of Lin and Pao. Calculations were performed on a grid with number of nodes 61 × 51 (grid No. 1). In the original plane (y,z), the nodes of the grid domain (y_i, z_j) were distributed as follows:

$$y_i = ih_{1y},\ i = 0,\ldots,30;\ y_i = y_{i-1}q_{1y},\ i = 31,\ldots,60,\ q_{1y} = 1.04;$$

$$z_j = jh_{1z},\ j = 0,\ldots,20;\ z_j = z_{j-1}q_{1z},\ j = 21,\ldots,50,\ q_{1z} = 1.047$$

($h_{1y} = h_{1z} = 0.1$). The value of Δx^n varied from 0.01 to 0.5 according to the formula for the sum of the terms of a arithmetical progression with difference 0.01.

To check the validity of the results given in Figs. 1–3, we also performed calculations on a finer grid with number of nodes 81 × 61 (grid No. 2):

$$y_i = ih_{2y},\ i = 0,\ldots,40;\quad y_i = y_{i-1}q_{2y},\ i = 41,\ldots,80,\ q_{2y} = 1.041;$$

TABLE 1

Grid	t	$\sqrt{e_0}$	ε_0	$\sqrt{\langle\rho_0'^2\rangle}$	U_{D0}	L_y	L_z	ψ_m
No. 1	0.5	$3.136 \cdot 10^{-2}$	$7.131 \cdot 10^{-5}$	$1.282 \cdot 10^{-1}$	$7.723 \cdot 10^{-2}$	$1.205 \cdot 10^{0}$	$1.195 \cdot 10^{0}$	$6.140 \cdot 10^{-4}$
No. 2		$3.174 \cdot 10^{-2}$	$7.153 \cdot 10^{-5}$	$1.289 \cdot 10^{-1}$	$7.404 \cdot 10^{-2}$	$1.203 \cdot 10^{0}$	$1.194 \cdot 10^{0}$	$6.355 \cdot 10^{-4}$
1	4.0	$6.655 \cdot 10^{-3}$	$3.614 \cdot 10^{-7}$	$3.256 \cdot 10^{-2}$	$2.344 \cdot 10^{-2}$	$1.581 \cdot 10^{0}$	$1.484 \cdot 10^{0}$	$2.757 \cdot 10^{-4}$
2		$6.660 \cdot 10^{-3}$	$3.551 \cdot 10^{-7}$	$3.261 \cdot 10^{-2}$	$2.223 \cdot 10^{-2}$	$1.583 \cdot 10^{0}$	$1.481 \cdot 10^{0}$	$2.473 \cdot 10^{-4}$

TABLE 2

t	I_{01}		U_{D0}		t	I_{01}		U_{D0}	
0.5	$6.95 \cdot 10^{-10}$	$-5.83 \cdot 10^{-4}$	$2.46 \cdot 10^{-2}$	$1.19 \cdot 10^{-2}$	6.0	$1.28 \cdot 10^{-8}$	$-6.92 \cdot 10^{-4}$	$3.99 \cdot 10^{-3}$	$-3.97 \cdot 10^{-5}$
2.0	$3.56 \cdot 10^{-9}$	$-6.90 \cdot 10^{-4}$	$6.43 \cdot 10^{-3}$	$8.61 \cdot 10^{-4}$	8.0	$1.48 \cdot 10^{-8}$	$-6.91 \cdot 10^{-4}$	$3.64 \cdot 10^{-3}$	$-1.29 \cdot 10^{-4}$
4.0	$9.12 \cdot 10^{-9}$	$-6.93 \cdot 10^{-4}$	$4.64 \cdot 10^{-3}$	$1.56 \cdot 10^{-4}$	10.0	$1.57 \cdot 10^{-8}$	$-6.91 \cdot 10^{-4}$	$3.40 \cdot 10^{-3}$	$1.80 \cdot 10^{-4}$

TABLE 3

Grid	t	$\sqrt{e_0}$	ε_0	$\sqrt{\langle\rho_0'^2\rangle}$	U_{D0}	L_y	L_z	ψ_m	E_t	P_t
No. 3	0.5	$4.09 \cdot 10^{-3}$	$6.28 \cdot 10^{-8}$	$5.80 \cdot 10^{-2}$	$1.60 \cdot 10^{-4}$	$1.58 \cdot 10^{0}$	$1.35 \cdot 10^{0}$	$2.54 \cdot 10^{-4}$	$1.28 \cdot 10^{-5}$	$3.04 \cdot 10^{-6}$
No. 4		$4.21 \cdot 10^{-3}$	$6.85 \cdot 10^{-8}$	$6.17 \cdot 10^{-2}$	$1.51 \cdot 10^{-4}$	$1.59 \cdot 10^{0}$	$1.31 \cdot 10^{0}$	$2.57 \cdot 10^{-4}$	$1.34 \cdot 10^{-5}$	$3.16 \cdot 10^{-6}$
3	4.0	$5.15 \cdot 10^{-4}$	$9.79 \cdot 10^{-11}$	$3.66 \cdot 10^{-2}$	$1.17 \cdot 10^{-5}$	$5.31 \cdot 10^{0}$	$1.02 \cdot 10^{0}$	$8.39 \cdot 10^{-4}$	$9.05 \cdot 10^{-7}$	$5.18 \cdot 10^{-6}$
4		$5.21 \cdot 10^{-4}$	$1.01 \cdot 10^{-10}$	$3.66 \cdot 10^{-2}$	$1.13 \cdot 10^{-5}$	$5.38 \cdot 10^{0}$	$0.96 \cdot 10^{0}$	$8.74 \cdot 10^{-4}$	$9.83 \cdot 10^{-7}$	$5.47 \cdot 10^{-6}$

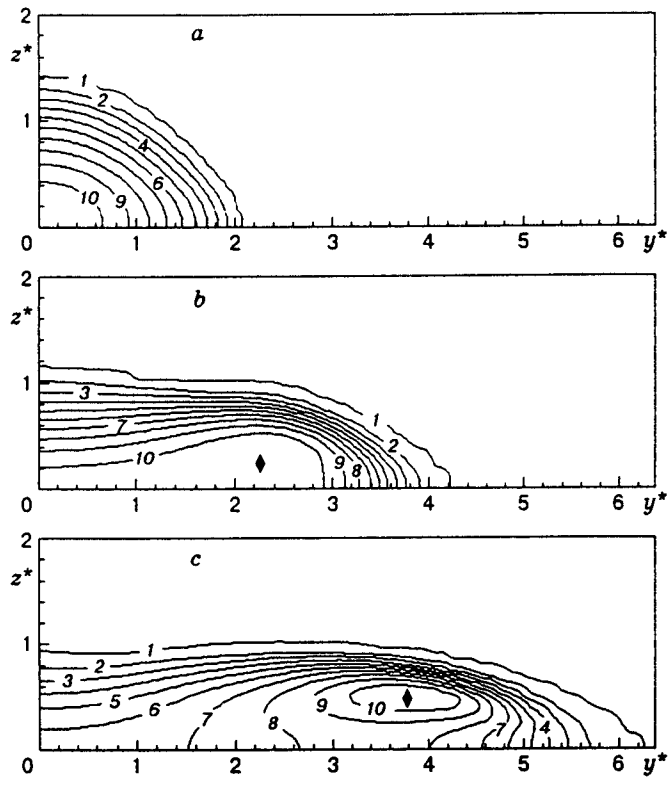

Fig. 4

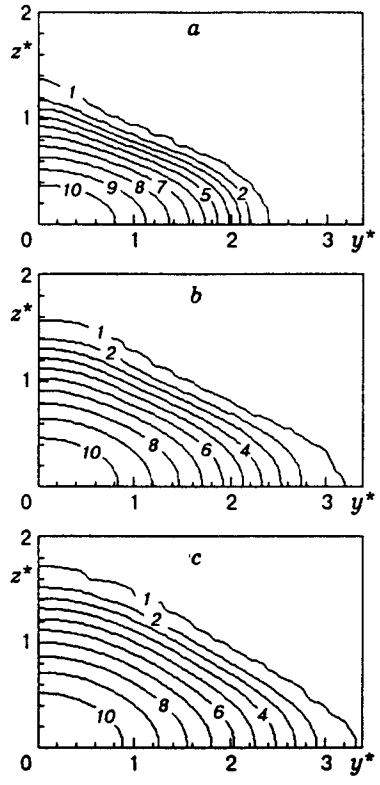

Fig. 5

$$z_j = jh_{2z},\ j = 0,\ldots,30; \quad z_j = z_{j-1}q_{2z},\ j = 31,\ldots,60,\ q_{2z} = 1.057$$

($h_{2y} = h_{1y}/2$ and $h_{2z} = h_{1z}/2$). The value of Δx^n varied here from 0.0025 to 0.15 according to the formula for the terms of an arithmetical progression with difference 0.0025 (here and below, the nondimensional grid parameters are given). Some data on comparison of the calculation results on grids No. 1 and 2 are presented in Table 1, where $\varepsilon_0 = \varepsilon_0(t) = \varepsilon(t,0,0)$, $\langle\rho_0'^2\rangle = \langle\rho'^2(t,0,0)\rangle$, $\psi_m = \psi_m(t) = \max\limits_{y_i,z_j}|\psi(t,y_i,z_j)|$, L_y and L_z are the characteristic vertical and horizontal sizes of the wake, respectively, which are determined from the relations $e(t,L_y,0) = 0.01e_0(t)$ and $e(t,0,L_z) = 0.01e_0(t)$. Note also that the deviations of the data arrays of grid values of the functions ψ, U_D, e, and ε did not exceed, in uniform norm, the deviations of the values presented in Table 1. This shows the reliability of the proposed algorithm. The data in Figs. 1–3 demonstrate the rather high efficiency of the mathematical model of turbulent wakes.

Let us analyze the role of the approximation of the boundary conditions on the axes of symmetry for Eq. (2.1). Table 2 lists the results of the numerical experiment performed on grid No. 1. The second and forth columns refer to the modified boundary conditions for Eq. (2.1), and columns 3 and 5 refer to the Neumann conditions for the longitudinal velocity-component defect. Approximation of the boundary conditions for (2.1) plays a very important part in U_{D0} variation.

5. Basic Calculation Results. The dynamics of a turbulent wake in a pycnocline is illustrated in Figs. 4, 6, 8a, and 9–11. Calculations were performed for the distribution of the nondimensional unperturbed-fluid density

$$\rho_{sn}(z) = \rho_s(z) = \widehat{\rho}_0 - \beta\tanh(z/\beta), \quad \widehat{\rho}_0 = 1/aD, \quad \beta = 0.1.$$

The Froude number was assumed to equal 565, which corresponds to the conditions of one of the laboratory experiments of Lin and Pao [3] in a linearly stratified medium. The initial conditions were specified in accordance with the experimental data of [3, 4] in a homogeneous fluid. Calculations were performed on

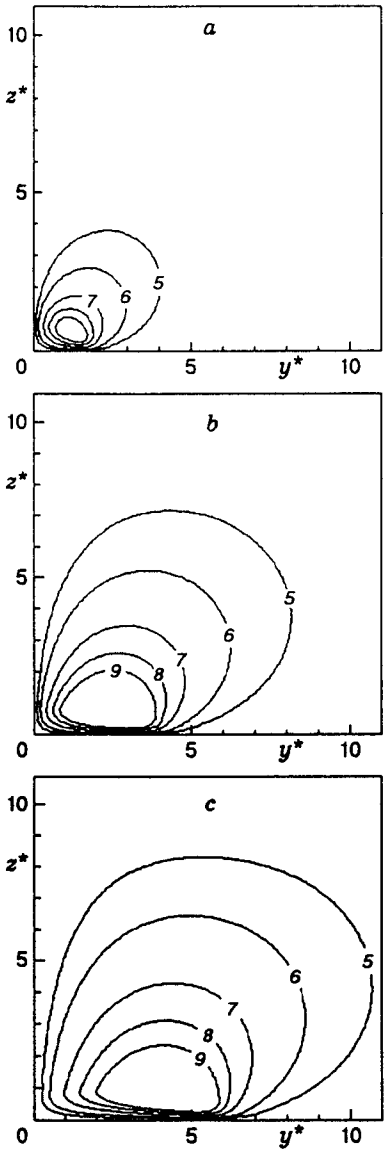

Fig. 6

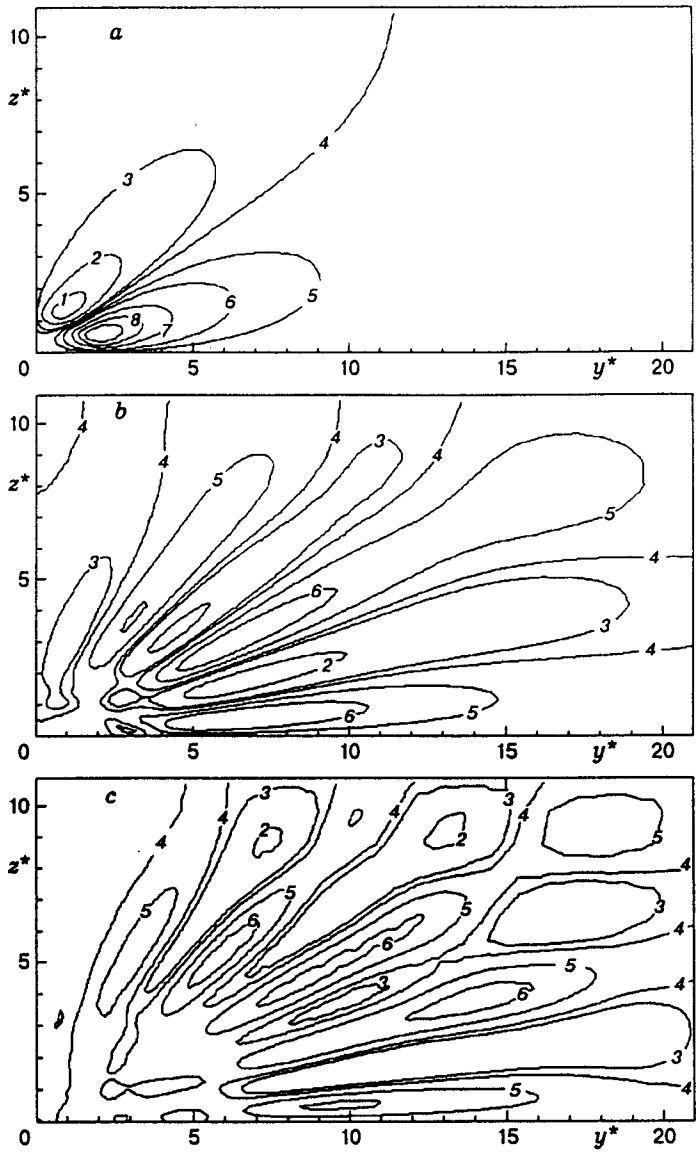

Fig. 7

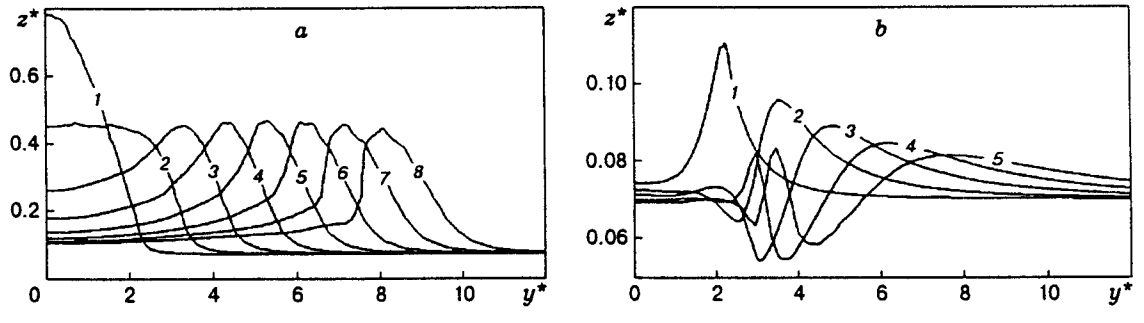

Fig. 8

TABLE 4

Model	t	$\sqrt{e_0}$	ε_0	$\sqrt{\langle\rho_0'^2\rangle}$	L_y	L_z	ψ_m	E_t
Complete	2.0	$1.12\cdot10^{-3}$	$1.02\cdot10^{-9}$	$5.03\cdot10^{-2}$	$3.15\cdot10^{0}$	$1.37\cdot10^{0}$	$8.37\cdot10^{-4}$	$1.96\cdot10^{-6}$
Simplified		$1.11\cdot10^{-3}$	$9.95\cdot10^{-10}$	$4.97\cdot10^{-2}$	$3.13\cdot10^{0}$	$1.34\cdot10^{0}$	$8.24\cdot10^{-4}$	$1.88\cdot10^{-6}$
Complete	5.0	$4.02\cdot10^{-4}$	$4.71\cdot10^{-11}$	$3.03\cdot10^{-2}$	$6.35\cdot10^{0}$	$0.94\cdot10^{0}$	$7.92\cdot10^{-4}$	$7.57\cdot10^{-7}$
Simplified		$3.97\cdot10^{-4}$	$4.58\cdot10^{-11}$	$3.05\cdot10^{-2}$	$6.32\cdot10^{0}$	$0.92\cdot10^{0}$	$7.79\cdot10^{-4}$	$7.27\cdot10^{-7}$
Complete	8.0	$2.51\cdot10^{-4}$	$1.14\cdot10^{-11}$	$1.92\cdot10^{-2}$	$9.09\cdot10^{0}$	$0.97\cdot10^{0}$	$6.24\cdot10^{-4}$	$5.02\cdot10^{-7}$
Simplified		$2.48\cdot10^{-4}$	$1.11\cdot10^{-11}$	$1.94\cdot10^{-2}$	$9.05\cdot10^{0}$	$0.96\cdot10^{0}$	$6.11\cdot10^{-4}$	$4.80\cdot10^{-7}$

a grid with 71 × 36 nodes (grid No. 3). In the plane (y, z), the nodes of the grid domain were distributed as follows:

$$y_i = ih_{3y},\ i = 0,\dots,30; \quad y_i = y_{i-1}q_{3y},\ i = 31,\dots,70,\ q_{3y} = 1.06;$$

$$z_j = jh_{3z},\ j = 0,\dots,10; \quad z_j = z_{j-1}q_{3z},\ j = 11,\dots,35,\ q_{3z} = 1.113$$

($h_{3y} = h_{3z} = 0.075$). The step Δx^n was varied from $\Delta x^0 = 0.055$ to 3.6 by the formula $\Delta x^{n+1} = \Delta x^n + 0.055$, and was further assumed to be constant.

Figures 4a–c show the curves of equal energy $e/e_m(t) = \text{const}$ and $e_m(t) = \max\limits_{y_i,z_j} e(t, y_i, z_j)$ for $t = 1$, 3, and 5, respectively; isolines 1–10 are presented by the levels 0.01, 0.1, 0.2, 0.3, 0.4, 0.5, 0.6, 0.7, 0.8, and 0.9; the point ♦ refers to the grid node in which a maximum of $e(t, y, z)$ is reached.

For comparison, Figs. 5a–c show the equal-energy curves for the linear density distribution of an unperturbed fluid (Fr = 565, the designations are the same as in Fig. 4).

Convective flow is illustrated in Figs. 6a–c and 7a–c where the streamlines with $\psi = \text{const}$ are plotted for $t = 1$, 3, and 5, respectively; isolines 1–9 correspond to the levels $-2\cdot10^{-4}$, -10^{-4}, $-2.5\cdot10^{-5}$, 0, $5\cdot10^{-5}$, 10^{-4}, $2\cdot10^{-4}$, $3\cdot10^{-4}$, and $4\cdot10^{-4}$. Clearly, there is a great difference in the dynamics of convective vortices for a pycnocline (Fig. 6) and for linear stratification (Fig. 7). Linear stratification is characterized by vortex subdivision and by the process of formation of opposite-direction vortices [23]. In the pycnocline considered, a single vortex which becomes practically a steady one for $t \geqslant 5$ is formed in each quadrant of the plane (y, z).

The decay of the turbulent wake is accompanied by generation of internal waves. Internal waves which are induced by the turbulent wake in the pycnocline are shown in Fig. 8a in which the dynamics of the curve $\hat{\rho}_0 - \langle\rho\rangle = \hat{\rho}_0 - \rho_{sn}(0, 07)$ is given for the moments of time $t = 1$, 2, 3, 4, 5, 6, 7, and 8 (curves 1–8). Evidently, for $t \geqslant 5$, the perturbation varies slightly, shifting virtually with constant velocity along the y axis.

The pattern of internal waves generated by the turbulent wake in a linearly stratified medium is illustrated in Fig. 8b where we show the dynamics of the curve $\hat{\rho}_0 - \langle\rho\rangle = \hat{\rho}_0 - \rho_{sl}(0, 07)$ for $t = 1$, 2, 3, 4, and 5 [(curves 1–5), $\rho_{sl}(z) = \hat{\rho}_0 - z$]. Unlike the pycnocline, the wave process is followed by the appearance of new crests and valleys with time. As a result, the flow in a linearly stratified medium is characterized by a considerably smaller amplitude of internal waves, this amplitude decreasing with time. The internal waves in Fig. 8 are in full agreement with the results of Figs. 6 and 7.

The decay of the turbulent wake is also shown in Figs. 9 and 10. Figure 9 shows the variation of the characteristic horizontal L_y (curves 1 and 3) and vertical L_z (curves 2 and 4) sizes of the turbulent wake. Curves 1 and 2 refer to the pycnocline, and curves 3 and 4 refer to the linearly stratified fluid. It is seen that the turbulent wake in the pycnocline spreads more intensely. At the same time, the variation in the turbulence energy on the axis of the wake $e_0(t)$ (see Fig. 10, where 1 is the pycnocline and 2 is the linear stratification) depends weakly on the type of stratification, although there are appreciable differences in the distributions of the $e = \text{const}$ curves (see Figs. 4 and 5). In the pycnocline, the maximum value of the turbulence energy for $t > 1.5$ is reached not on the wake axis, which is explained by the specific features of the dynamics of the averaged convective motion caused by the wake collapse (see Figs. 6–8).

We shall dwell on the estimates of the calculational accuracy. The basic calculations were carried out

TABLE 5

t	$\delta\rho$		$\delta\psi$	
5	0.184	0.095	0.090	0.031
6	0.196	0.162	0.140	0.085
7	0.194	0.168	0.178	0.134
8	0.254	0.205	0.208	0.168

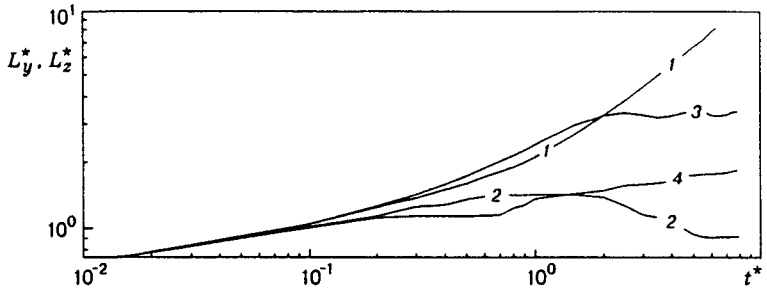

Fig. 9

on grid No. 3. We also made calculations on a finer grid (grid No. 4) which was arranged similarly to grid No. 3 in the horizontal direction, and the nodes in the vertical direction were distributed in the following manner:

$$z_j = jh_{4z},\ j = 0,\dots,20; \quad z_j = z_{j-1}q_{4z},\ j = 21,\dots,55,\ q_{4z} = 1.082$$

($h_{4z} = 0.035$). The step Δx^n (similarly to grid No. 3) was varied from 0.015 to 0.9.

Some data obtained by comparing the pycnocline calculations on grids Nos. 3 and 4 are given in Table 3. Clearly, the calculation results are sufficiently close. The deviations of the data arrays of the desired functions in a norm that is a grid analog of the space norm of continuous functions did not exceed the deviations of the characteristic wake parameters given in Table 3.

6. Simplified Models. The fact that the defect of the longitudinal velocity component U_D degenerates much more rapidly than $\sqrt{e}$ is the known result of calculational-theoretical and experimental studies [36, 37] of the dynamics of momentumless turbulent wakes in a homogeneous fluid. In this connection, the mathematical model of the momentumless turbulent wake in a pycnocline in which $U_D \equiv 0$ is of interest.

Some calculation results with application of the complete ($U_D \neq 0$) and simplified ($U_D \equiv 0$) models are presented in Table 4. Numerical experiments were performed using grid No. 3. The calculation results can be considered rather close.

Further simplification of the mathematical flow model is connected with analysis of the behavior of the total turbulence $E_t(t)$ and internal-wave $P_t(t)$ energies:

$$E_t(t) = \int_0^\infty\!\!\int e\,dy\,dz \equiv \int_0^\infty\!\!\int eJ\,d\xi\,d\eta, \quad P_t(t) = \int_0^\infty\!\!\int \left(\frac{V^2+W^2}{2} + \frac{4\pi^2}{\mathrm{Fr}^2}\langle\rho_1\rangle z\right) J\,d\xi\,d\eta.$$

Variation of these quantities as a function of time is shown in Fig. 11 where curves 1 and 2 corresponds to $E_t(t)$ and $P_t(t)$ in the pycnocline, and curves 3 and 4 correspond to $E_t(t)$ and $P_t(t)$ in a linearly stratified fluid. Evidently, the $E_t(t)$ value decreases monotonically with time (curves 1 and 3) owing to dissipation of the turbulent energy into heat under the action of molecular viscosity. At the same time, owing to diffusion of the turbulent mass and the work of buoyancy forces, a portion of the turbulence energy becomes potential, generation of internal wave begins, and $P_t(t)$ increases up to $t \approx 3$ (curves 2 and 4). For large values of time, $P_t(t)$, however, remains practically constant. Just as in the case of a model problem on the dynamics of the localized zone of turbulent mixing [26, 29], such a behavior of $P_t(t)$ and $E_t(t)$ shows flow splitting into the wave and diffusion processes.

The latter allows one to propose simplified mathematical models for calculation of the dynamics of the far turbulent wake: the Euler equations in the Boussinesq approach for numerical modeling of the characteristics of internal waves, and the diffusion model for numerical analysis of the characteristics of the turbulent wake proper. Some calculation results which demonstrate the possibility of applying a simplified model (Euler equations in the Boussinesq approximation) to computation of internal waves generated by the

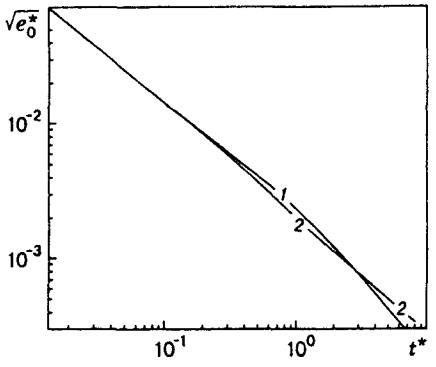

Fig. 10

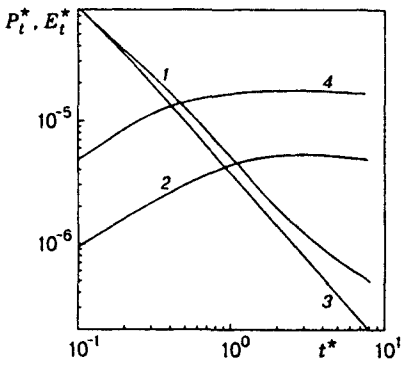

Fig. 11

far turbulent wake are listed in Table 5, where

$$\delta\rho = \max_{i,j} |\langle\rho_1\rangle_{i,j}^{n_0} - \langle\widehat{\rho}_1\rangle_{i,j}^{n_0}| / \max\{|\langle\rho_1\rangle_{i,j}^{n_0}|, |\langle\widehat{\rho}_1\rangle_{i,j}^{n_0}|\},\ \delta\psi = \max_{i,j} |\psi_{i,j}^{n_0} - \widehat{\psi}_{i,j}^{n_0}| / \max_{i,j}\{|\psi_{i,j}^{n_0}|, |\widehat{\psi}_{i,j}^{n_0}|\}.$$

Here the hat symbol denotes quantities obtained using the simplified model; the time-layer number n_0 is chosen such that the time values correspond to those given in Table 5. The second and fourth columns show the results of comparison of the computational data obtained by the complete and simplified models when the initial conditions for the latter model were set based on the solution of the complete problem for $t = 3$. For comparison, the third and fifth columns show the data of computations in which the simplified model was employed for $t \geqslant 4$. Application of the diffusion model for $t \geqslant 3$ gives rise, in particular, to deviations (compared with the complete model) which differ by not greater than 20% from the axial values of the turbulence energy.

The deviations in Table 5 substantially exceed those which correspond to the case of a linear stratification [20, 21]. This is caused by the presence, in pycnocline, of a weak interaction of the turbulence in the wake and the wake-induced wave motions. This interaction is nevertheless not intense, and it is expedient to use the simplified models for numerical flow analysis.

Let us go over again to the results in Fig. 8a. Since the problem on the dynamics of internal waves generated by the collapse of the turbulent wake in the pycnocline can be regarded as the Cauchy problem for the Euler equations in the Boussinesq approximation, it is natural to attempt to estimate the parameters of these waves with the use of the asymptotic relation in [38] which relates the maximum amplitude $\bar{A}$ to the wave velocity $\bar{c}$:

$$(\bar{c})^2 = \frac{\beta^2}{2}\left(1 + \frac{3}{5}\frac{\bar{A}}{\beta}\right). \tag{6.1}$$

As follows from the computations, $\bar{c} = cT_*/D = 0.15$, $T_* = 1/\sqrt{ag}$, and $\bar{A} = A/D = 0.39$. For $\bar{A} = 0.39$, relation (6.1) yields $\bar{c}_a = 0.13$ which points to, precisely as in [5], the possibility of applying relation (6.1) to approximate estimates.

Thus, we have constructed a numerical model of the dynamics of a momentumless turbulent wake in a pycnocline. We have also considered a simple modified e–ε model of turbulence and the equally simple (but reliable enough) finite-difference algorithm of solution. Improving the mathematical model and its discrete analog is the subject of further studies.

This work was supported by the Russian Foundation for Fundamental Research (Grant Nos. 93-01-17925 and 95-01-00910).

REFERENCES

1. A. H. Schooley and R. W. Stewart, "Experiments with a self-propelled body submerged in a fluid

with vertical density gradient," *J. Fluid Mech.*, **15**, No. 1, 83–96 (1963).
2. G. E. Merrit, "Wake growth and collapse in stratified flow," *AIAA J.*, **12**, No. 7, 940–949 (1974).
3. J. T. Lin and Y. H. Pao, "Wakes in stratified fluids," *Ann. Rev. Fluid Mech.*, **11**, 317–336 (1979).
4. S. Hassid, "Collapse of turbulent wakes in stable stratified media," *J. Hydronautics*, **14**, No. 1, 25–32 (1980).
5. H. E. Gilreath and A. Brandt, "Experiments on the generation of internal waves in a stratified fluid," *AIAA J.*, **23**, 693–700 (1985).
6. E. Ya. Sysoyeva and Yu. D. Chashechkin, "Vortex structure of the wake behind a sphere in a stratified fluid," *Prikl. Mekh. Tekh. Fiz.*, No. 2, 40–46 (1986).
7. E. J. Hopfinger, J. B. Flor, J. M. Chomaz, and P. Bonneton, "Internal waves generated by a moving sphere and its wake in stratified fluid," *Exp. Fluids*, **11**, 255–261 (1991).
8. Q. Lin, D. L. Boyer, and J. S. Fernando, "Turbulent wakes of linearly stratified flow past a sphere," *Phys. Fluids A*, **4**, No. 8, 1687–1696 (1992).
9. J. M. Chomas, P. Bonneton, A. Butet, and E. J. Hopfinger, "Vertical diffusion of the far wake of a sphere moving in a stratified fluid," *Phys. Fluids A*, **5**, No. 11, 2799–2806 (1993).
10. P. Bonneton, J. M. Chomas, and E. J. Hopfinger, "Internal waves produced by the turbulent wake of a sphere moving horizontally in a stratified fluid," *J. Fluid Mech.*, **254**, 23–40 (1993).
11. O. D. Shishkina, "Influence of wake regimes on the hydrodynamic characteristics of a submerged sphere in a stratified fluid," in: Preprints of the 4th Int. Symp. on Stratified Flows, Grenoble Inst. of Mech., Grenoble (1994), Vol. 3, sess. A5, No. 39.
12. Yu. D. Chashechkin. "Internal waves, vortices and turbulence in a wake past a bluff body in a continuously stratified liquid," *ibid.*, Vol. 2, sess. B4, No. 29 (1994).
13. G. R. Spedding, F. K. Browand, and A. M. Fincham, "The structure and long-time evolution of bluff body wakes in a stable stratification," *ibid.*, Vol. 2, sess. B4, No. 196 (1994).
14. B. Voisin, "Rayonnement des ondes internes de gravite. Application aux corps en mouvement," Ph.D. thesis, University Pierre et Marie Curie (1991).
15. A. T. Onufriev, "Turbulent wake in a stratified medium," *Prikl. Mekh. Tekh. Fiz.*, No. 5, 68–72 (1970).
16. W. S. Lewellen, M. E. Teske, and C. Dup. Donaldson, "Examples of variable density flows computed by second-order closure description of turbulence," *AIAA J.*, **14**, 382–387 (1976).
17. A. Yu. Danilenko, V. I. Kostin, and A. I. Tolstykh, "An implicit algorithm of computation of flows of a homogeneous and nonhomogeneous fluid," Preprint, Computing Center, USSR Academy of Sci., Moscow (1985).
18. G. G. Chernykh, N. N. Fedorova, and N. P. Moshkin, "Numerical simulation of turbulent wakes," *Russ. J. Theoret. Appl. Mech.*, **2**, 295–304 (1992).
19. G. S. Glushko, A. G. Gumilevskii, and V. I. Polezhayev, "Evolution of turbulent wakes behind sphere-shaped bodies in stably stratified media," *Izv. Ross. Akad. Nauk, Mekh. Zhidk. Gaza*, No. 1, 13–22 (1994).
20. G. G. Chernykh, N. P. Moshkin, and O. F. Voropayeva, "Turbulent wakes in stratified fluids: results of numerical experiments," in: *Preprints of the 4th Int. Symp. on Stratified Flows*, Grenoble Inst. of Mech., Grenoble (1994), Vol. 1, sess. A2, No. 103.
21. G. G. Chernykh, N. P. Moshkin, and O. F. Voropayeva, "Numerical models of momentumless turbulent wakes in stratified media," in: *Proc. of the 7th Int. Conf. on the Meth. of Aerophys. Res.* [in Russian]. Inst. Theor. Appl. Mech., Novosibirsk, Part 1, pp. 58–63 (1994).
22. J. A. Shetz, *Injection and Mixing in Turbulent Flow*, Am. Inst. of Aeronautics and Astronautics, New York (1980).
23. O. F. Vasil'ev, B. G. Kuznetsov, Yu. M. Lytkin, and G. G. Chernykh, "Development of the turbulent-fluid region in a stratified medium," in: Int. Symp. on Stratified Flows, Novosibirsk (1972).
24. A. M. Trokhan and Yu. D. Chashechkin, "Generation of internal waves in a stratified fluid by a pulsed hydrodynamically linear source (two-dimensional problem)," in: *Theory of Wave Diffraction*

and Propagation [in Russian]: Brief Abstracts at the 7th All-Union Symp. on Wave Diffraction and Propagation, Rostov-on-Don (1977), Vol. 3, pp. 186–189.

25. T. W. Kao and H. P. Pao. "Wake collapse in the thermocline and internal solitary waves," *J. Fluid Mech.*, **97**, No. 1, 115–127 (1980).
26. G. G. Chernykh, Y. M. Lytkin, and I. V. Sturova, "Numerical simulation of internal waves induced by the collapse of turbulent mixed region in a stratified medium," in: Proc. of Int. Symp. on Refined Modeling of Flows, 7–10 Sept., Paris (1982), pp. 671–679.
27. V. A. Popov, "Development of the region of a partially mixed fluid in a thin-laminated stratified medium," *Izv. Akad. Nauk SSSR, Fiz. Atmos. Okeana*, **22**, No. 4, 389–394 (1986).
28. G. G. Chernykh, O. F. Filippova, and A. N. Zudin, "Evolution of local density perturbation in stratified medium: results of numerical experiments," in: *Proc. of the 1st Soviet Union–Jpn. Symp. on Computational Fluid Dynamics*, Khabarovsk, Sept. 9–16, 1988 [in Russian], Computing Center of the USSR Acad. Sci., Moscow (1989), Part 1, pp. 128–133.
29. O. F. Voropayeva and G. G. Chernykh, "Evolution of the turbulent-mixing zone in a fluid with nonlinear stratification," in: *Simulation in Mechanics* (Collected scientific papers) [in Russian], **3(20)**, No. 5, Computing Center–Inst. of Theor. And Applied Mechanics, Novosibirsk (1989), pp. 3–29.
30. J. B. Flor, H. J. S. Fernando, and G. J. F. Heijst, "The evolution of an isolated turbulent region in a two-layer fluid," *Phys. Fluids*, **6**, No. 1, 287–296 (1994).
31. L. I. Skurin, "Quasi-one-dimensional model of the evolution of a turbulent wake region behind a body in a stratified medium," *Izv. Akad. Nauk SSSR, Fiz. Atmos. Okeana*, **22**, No. 4, 373–379 (1986).
32. W. Rodi, "Examples of calculation methods for flow and mixing in stratified fluids," *J. Geoph. Res.*, **92**, No. C5, 5305–5328 (1987).
33. N. N. Yanenko, *Method of Fractional Steps for Solution of Multidimensional Problems of Mathematical Physics* [in Russian], Nauka, Novosibirsk (1967).
34. A. G. Demenkov and G. G. Chernykh, "Numerical simulation of jet flows of a viscid incompressible fluid," in: *Computational Technologies* (Collected scientific papers) [in Russian], **4**, No. 12, Inst. of Comp. Technologies, Novosibirsk (1995), pp. 119–131.
35. A. A. Samarskii and I. M. Sobol', "Examples of calculation of temperature waves," *Zh. Vychisl. Mat. Mat. Fiz.*, **3**, No. 4, 702–719 (1963).
36. V. A. Sabel'nikov, "Some specific features of turbulent flows with zero excess momentum," *Uch. Zap. TsAGI*, **6**, No. 4, 71–74 (1975).
37. N. V. Alekseenko and V. A. Kostomakha, "Experimental study of the dynamics of momentumless turbulent jet flow," *Prikl. Mekh. Tekh. Fiz.*, No. 1, 65–69 (1987).
38. T. B. Benjamin, "Internal waves of permanent form in fluids of great depth," *J. Fluid Mech.*, **29**, No. 3, 559–592 (1967).